Journal of Power Sources 196 (2011) 7692–7699

Contents lists available at ScienceDirect

Journal of Power Sources

journal homepage: www.elsevier.com/locate/jpowsour

Fabrication and electrochemical characteristics of electrospun $LiFePO_4$/carbon composite fibers for lithium-ion batteries

Ozan Toprakci, Liwen Ji, Zhan Lin, Hatice A.K. Toprakci, Xiangwu Zhang*

Fiber and Polymer Science Program, Department of Textile Engineering, Chemistry and Science, North Carolina State University, 2401 Research Drive, Raleigh, NC 27695-8301, USA

ARTICLE INFO

Article history:
Received 10 March 2011
Received in revised form 14 April 2011
Accepted 15 April 2011
Available online 22 April 2011

Keywords:
$LiFePO_4$
Cathodes
Fibers
Electrospinning
Lithium-ion batteries

ABSTRACT

$LiFePO_4$/C composite fibers were synthesized by using a combination of electrospinning and sol–gel techniques. Polyacrylonitrile (PAN) was used as an electrospinning media and a carbon source. $LiFePO_4$ precursor materials and PAN were dissolved in N,N-dimethylformamide separately and they were mixed before electrospinning. $LiFePO_4$ precursor/PAN fibers were heat treated, during which $LiFePO_4$ precursor transformed to energy-storage $LiFePO_4$ material and PAN was converted to carbon. The surface morphology and microstructure of the obtained $LiFePO_4$/C composite fibers were characterized using scanning electron microscopy (SEM), transmission electron microscopy (TEM) and elemental dispersive spectroscopy (EDS). XRD measurements were also carried out in order to determine the structure of $LiFePO_4$/C composite fibers. Electrochemical performance of $LiFePO_4$/carbon composite fibers was evaluated in coin-type cells. Carbon content and heat treatment conditions (such as stabilization temperature, calcination/carbonization temperature, calcination/carbonization time, etc.) were optimized in terms of electrochemical performance.

1. Introduction

Among various alternative cathode materials, lithium iron phosphate ($LiFePO_4$), which was discovered by Goodenough in 1997 [1], is gaining significant attention because of its relatively low cost, high discharge potential (very flat voltage curve around 3.4 V versus Li/Li^+), large specific capacity (170 mAh g^{-1}), good thermal stability, excellent cycling performance, low toxicity, and safe nature. However, $LiFePO_4$ has low conductivity ($\sim 10^{-9}$ S cm^{-1}), which leads to high impedance and low rate capability for batteries using that material [2]. In order to overcome this problem, different approaches can be used including doping $LiFePO_4$ with metal ions [2–4], coating with carbonaceous materials [5–7], and reducing the particle size [8], etc.

$LiFePO_4$ is typically prepared by both solid-state and solution-based methods, which have been reviewed elsewhere [9,10]. In this study, a different and promising approach, *i.e.*, electrospinning, was used to obtain $LiFePO_4$/C composite fibers that have high conductivity and excellent electrochemical performance. Electrospinning is an effective way of producing fibers from polymer solution by using an electrical force. Electrospun fibers have been investigated for use in lithium-ion battery applications including cathodes [11,12], separators [13] and anodes [14]. Here, we present the preparation, morphology, and electrochemical performance of electrospun $LiFePO_4$/C composite fiber cathodes for lithium-ion batteries.

2. Experimental

2.1. Sample preparation

Electrospun $LiFePO_4$/C composite fibers were produced as cathode materials for lithium-ion batteries. Spinning solutions consisted of polyacrylonitrile (PAN, Pfaltz & Bauer Inc., 150,000 g mol^{-1}) and $LiFePO_4$ precursor. PAN was used as the carbon source because it has high dielectric constant, which is crucial for electrospinning, and is a good source for carbon nanofibers [15,16]. PAN was first dissolved in N,N-dimethylformamide (DMF, Aldrich) at room temperature by stirring for 24 h. For $LiFePO_4$ precursor, lithium acetate ($LiCOOCH_3$, Aldrich), phosphoric acid (H_3PO_4, Aldrich) and iron (II) acetate ($Fe(COOCH_3)_2$, Aldrich) were used as the starting materials and mixed in DMF at a stoichiometric ratio of 1:1:1 by stirring at room temperature for 24 h. Separately prepared PAN and $LiFePO_4$ precursor solutions were then mixed with different ratios to obtain electrospinning solutions. Table 1 shows the concentrations of PAN, $LiFePO_4$ precursor and DMF in the obtained electrospinning solutions (S1, S2, and S3). The PAN concentration was determined by taking into consideration of the spinnability of $LiFePO_4$ precursor/PAN mixed solutions and the carbon content in the resultant $LiFePO_4$/C composite fibers. A

* Corresponding author. Tel.: +1 919 515 6547; fax: +1 919 515 6532.
E-mail address: xiangwu_zhang@ncsu.edu (X. Zhang).

0378-7753/$ – see front matter © 2011 Elsevier B.V. All rights reserved.
doi:10.1016/j.jpowsour.2011.04.031

Table 1
Concentrations of PAN, $LiFePO_4$ precursor and solvent in electrospinning solutions.

Sample ID	PAN (wt%)	$LiFePO_4$ precursor (wt%)	Solvent (DMF) (wt%)
S1	4	4	92
S2	4	8	88
S3	4	12	84

schematic diagram of the overall experimental procedure is shown in Fig. 1.

Electrospinning solutions were placed in 10 ml syringes with metal needles of 0.012 in. in diameter. A power supply (ES40P-20W/DAM) was used to provide a high voltage (15 kV). Needle-to-collector distance was set as 15 cm and electrospun fibers were collected on an aluminum foil. Electrospun $LiFePO_4$ precursor/PAN fibers were heat treated in two steps as shown in Fig. 2a. In the first step, fibers were stabilized under air. The process started at room temperature and reached 200, 240 or 280 °C with an increment rate of 5 °C min^{-1}. That temperature was maintained for 5 h to complete the stabilization process, during which the cyano side groups of PAN form cyclic rings mainly by a dehydrogenation process (Fig. 2b) [17]. In the second step, fibers were calcined and carbonized at 600, 700 or 800 °C for different times under argon atmosphere. During calcination/carbonization, $LiFePO_4$ precursor transformed to energy-storage $LiFePO_4$ material and PAN became electrically conducting carbon (Fig. 2c). The unique aspect of this process is that PAN was not only used as an electrospinning media for providing the spinnability of $LiFePO_4$ precursor/PAN composite fibers but also as a carbon source in order to increase the conductivity of $LiFePO_4$. Unlike in previous studies such as mixing or coating $LiFePO_4$ with a conducting material, here, conductive coating and $LiFePO_4$ formation take place at the same time during heat treatment, which ensures nano-scale

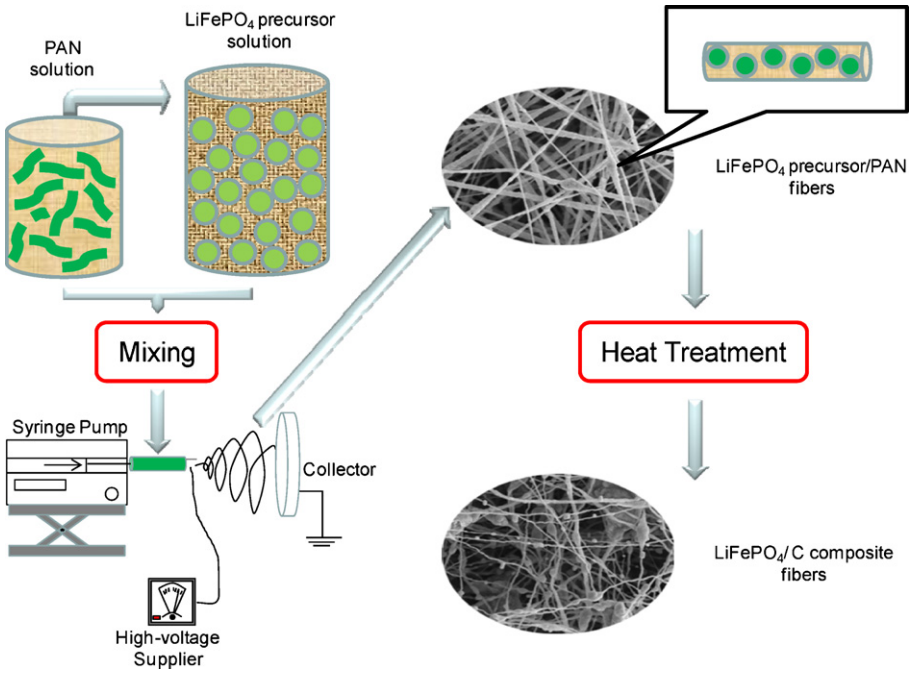

Fig. 1. Schematic diagram of experimental procedure.

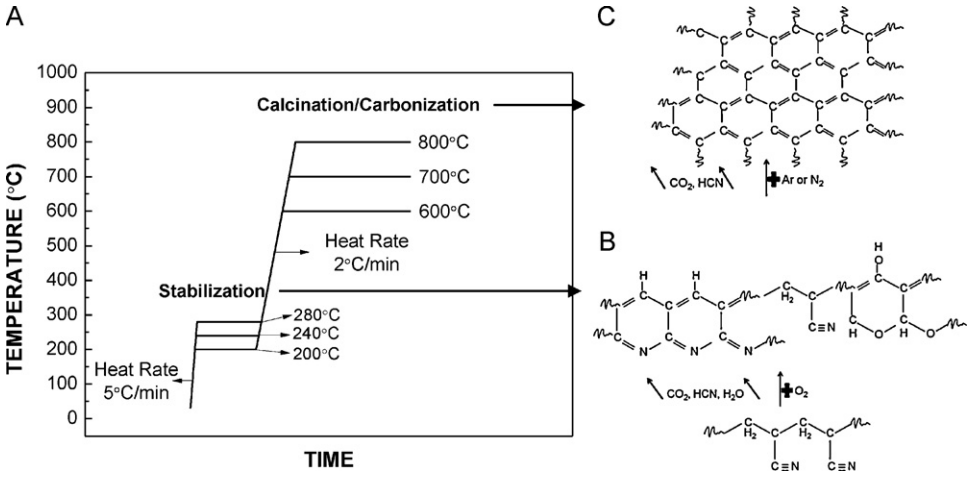

Fig. 2. Heat treatment of $LiFePO_4$ precursor/PAN fibers (a), and stabilization (b) and carbonization (c) of PAN.

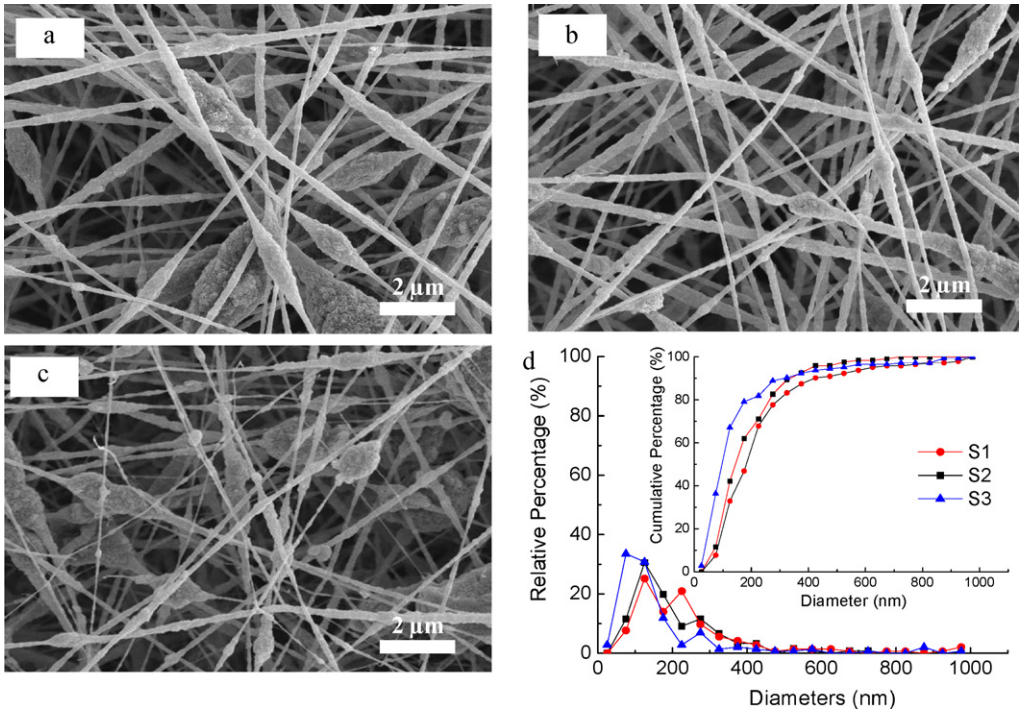

Fig. 3. SEM images of $LiFePO_4$ precursor/PAN fibers electrospun from S1 (a), S2 (b), S3 (c), and their diameter distributions (d).

carbon coating on the particle surface and maximizes $LiFePO_4$–carbon interface.

2.2. Structure characterization

The morphology and diameter of electrospun fibers and their heat-treated products were evaluated by using field emission scanning electron microscope (FESEM-JEOL 6400F SEM at 5 kV). The microstructure of heat-treated $LiFePO_4$/C composite fibers was observed using transmission electron microscope (Hitachi HF2000 TEM at 200 kV). TEM samples were ultrasonically treated in a solution of ethanol and then deposited on 200-mesh copper grids coated with carbon. The elemental distribution in $LiFePO_4$/C composite fibers was confirmed with elemental dispersive spectroscope (Oxford Isis EDS System). The structural characterization of $LiFePO_4$/C composite fibers was carried out by wide-angle X-ray

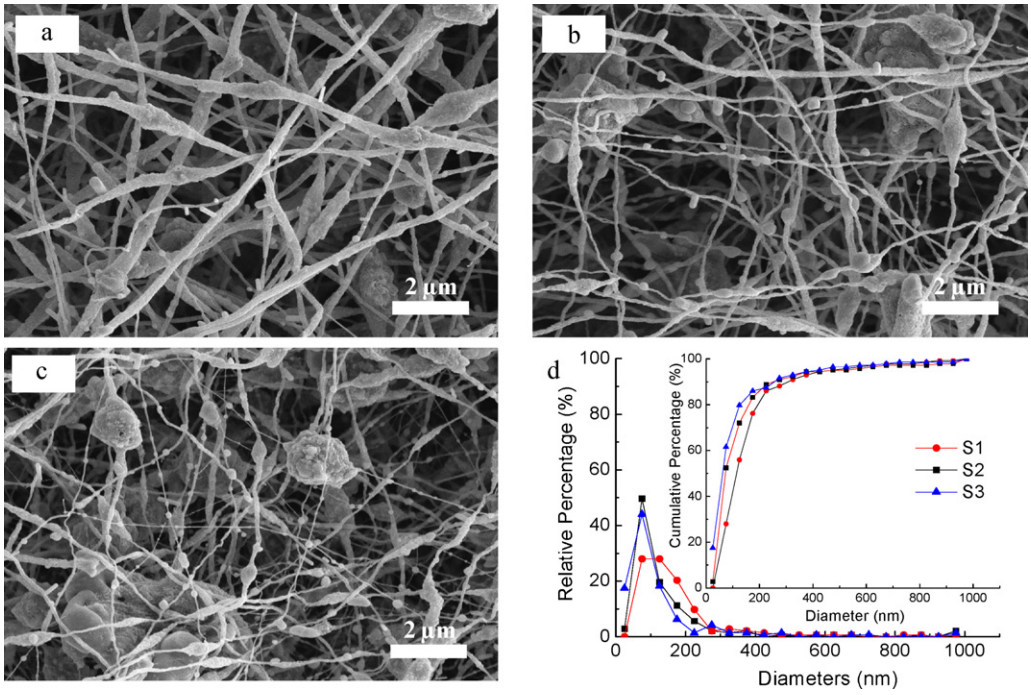

Fig. 4. SEM images of $LiFePO_4$/C composite fibers prepared from S1 (a), S2 (b), S3 (c) and their diameter distributions (d).

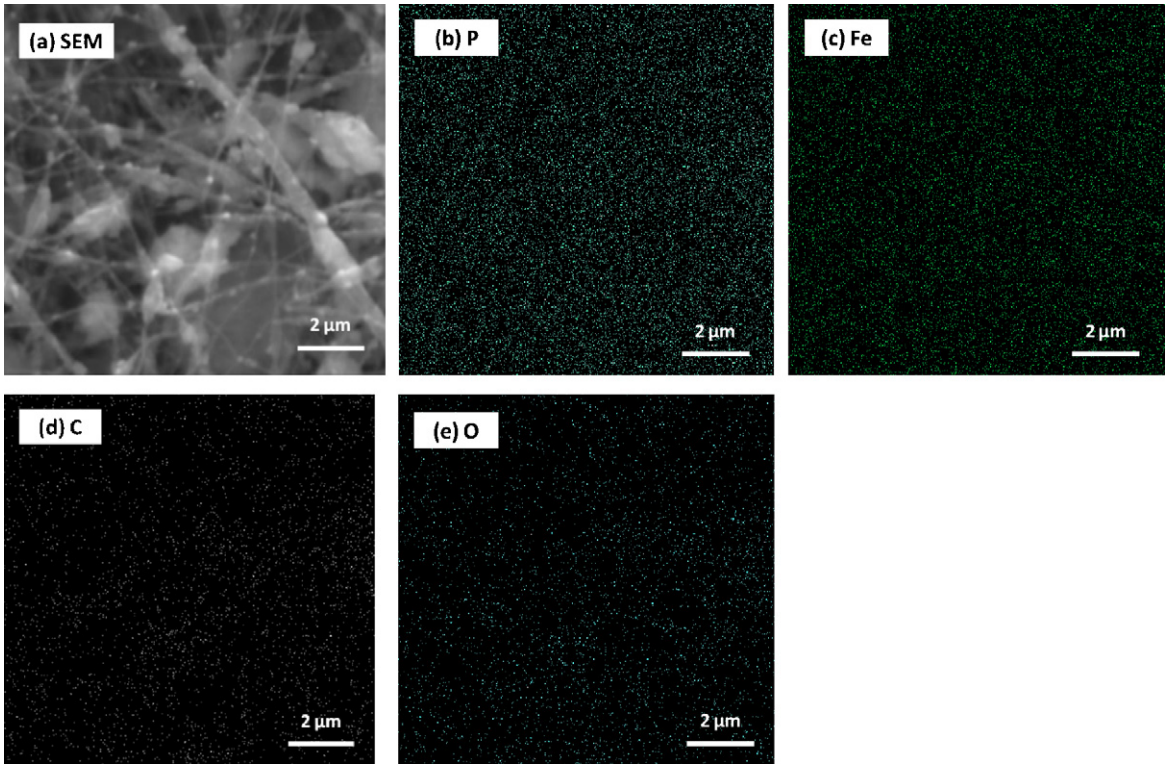

Fig. 5. SEM image (a) and corresponding EDS maps of phosphorus (b), iron (c), carbon (d) and oxygen (e) in $LiFePO_4$/C composite fibers prepared from S2.

diffraction (WAXD, Philips X'Pert PRO MRD HR X-Ray Diffraction System, Cu Kα, λ = 1.5405 Å) in a 2θ range of 15–90°, with 2θ step-scan intervals of 0.05°. The carbon amounts of composite fibers were determined by elemental analysis (Perkin Elmer 2400 Series II CHNS/O Elemental Analyzer).

2.3. Electrochemical measurements

$LiFePO_4$/C composite fibers have a tap density of around 1 g cm^{-3} and they were directly used as the cathode without adding any polymer binder or conductive material. CR2032-type coin cells (diameter = 20 mm and height = 3.2 mm) were fabricated using lithium metal as a counter electrode in an argon-filled glove box. The cathode weight was around 2.5 mg per electrode. The electrolyte used consisted of a 1 M solution of $LiPF_6$ in a mixture (1:1 by volume) of ethylene carbonate (EC) and ethyl methyl carbonate (EMC). The separator (Celgard 2400) was soaked in the electrolyte for 24 h prior to testing. The charge and discharge characteristics of the cathode were evaluated at various current rates (0.05–2 C, 1 C = 170 mA g^{-1}) in the range of 2.5–4.2 V versus Li/Li^+. All electrochemical experiments were conducted at room temperature and all capacity values were calculated based on the weight of active material $LiFePO_4$.

3. Results and discussion

3.1. Morphology of $LiFePO_4$ precursor/PAN and $LiFePO_4$/C composite fibers

Since the morphology and particle size of $LiFePO_4$ cathodes have great influence on their electrochemical performance [18], SEM analyses of electrospun $LiFePO_4$ precursor/PAN and heat-treated $LiFePO_4$/C composite fibers were carried out, and results are shown in Figs. 3 and 4. The conditions used for heat-treating the fibers were: stabilization at 280 °C for 5 h and calcination/carbonization at 700 °C for 18 h.

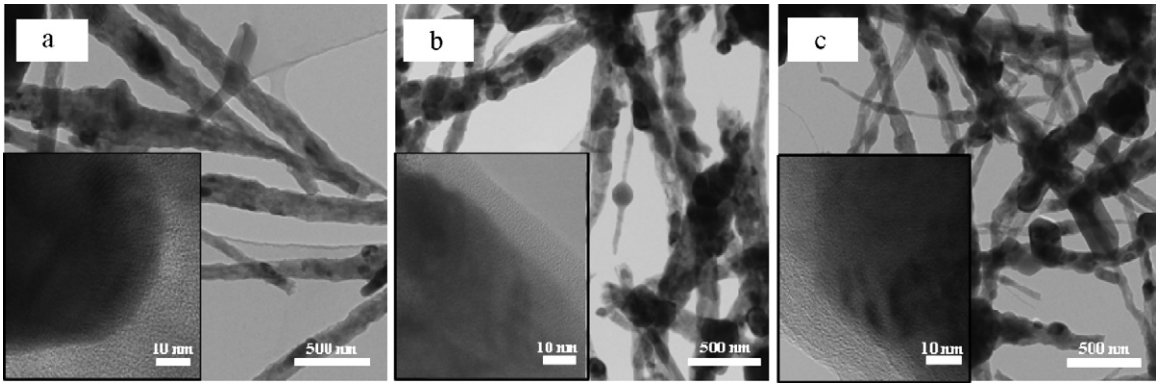

Fig. 6. TEM images of electrospun $LiFePO_4$/C composite fibers prepared from S1 (a), S2 (b) and S3 (c).

It is seen from Fig. 3 that for all three samples, electrospun fibers form "network-like" structures. At the same time, variations in the fiber diameters are observed and beads are also formed. As shown in Fig. 3d, with increase in $LiFePO_4$ precursor concentration, the average fiber diameter of electrospun $LiFePO_4$ precursor/PAN fibers decreases (*i.e.*, $D_{S1} > D_{S2} > D_{S3}$).

The diameter distributions of electrospun fibers were calculated using the following equation: $[D_{90} - D_{10}]/D_{50}$, where D_{10}, D_{50}, and D_{90} are fiber diameters at which 10%, 50% and 90% of fibers are finer than, respectively. A lower distribution value indicates higher homogeneity. The distribution values of fibers electrospun from S1, S2, and S3 were calculated to be 1.7, 1.8, and 2.4, respectively, indicating that the fibers become less uniform when $LiFePO_4$ precursor concentration increases.

Heat treatment has influence on the morphology of electrospinning fibers. Comparing Figs. 3 and 4, it is seen that after heat treatment, the fiber structure is still maintained; however, more beads are formed. In addition, substantial fiber diameter decrease is observed because of the removal of some species (such as CO_2, HCN, and NH_3, etc.) from the structure during heat treatment. Average diameter of heat-treated $LiFePO_4$/C fibers follows the same trend as electrospun fibers ($D_{S1} > D_{S2} > D_{S3}$). In addition, higher $LiFePO_4$ precursor concentration leads to higher distribution value (*i.e.*, 2.0, 2.2, and 3.2 for fibers prepared from S1, S2, and S3, respectively).

The carbon contents of heat-treated $LiFePO_4$/C composite fibers were measured using elemental analysis and they are 22.5, 17.0, and 14.3 wt%, respectively, for fibers prepared from S1, S2, and S3. Fig. 5 shows a SEM image of $LiFePO_4$/C composite fibers (prepared from S2) and its corresponding EDS maps of phosphorous, iron, carbon, and oxygen (Li cannot be observed by EDS). Uniform element distribution of iron, phosphorous and oxygen throughout the sample can be seen clearly.

In addition to SEM and EDS analyses, further evaluation was carried out by TEM in order to determine the particle microstructure and carbon coating characteristics. Fig. 6 shows TEM images of $LiFePO_4$/C composite fibers prepared from S1, S2, and S3. Fibers prepared from S2 and S3 showed relatively higher $LiFePO_4$ content compared with those from S1. This is consistent with the carbon content data measured by elemental analysis. $LiFePO_4$/C composite fibers prepared from S2 and S3 have lower carbon contents (17.0 and 14.3 wt%) and they have thinner carbon coatings of 8 and 12 nm, respectively (see magnified TEM images in Fig. 6b and c). On the other hand, it is observed that fibers prepared from S1 have a carbon content of 22.5 wt% and show a carbon coating thickness of more than 15 nm (Fig. 6a).

3.2. Structure characteristics of $LiFePO_4$/C composite fibers

Fig. 7a shows the XRD patterns of $LiFePO_4$/C composite fibers prepared from three electrospinning solutions (S1, S2, and S3). For comparison, the XRD pattern of pristine $LiFePO_4$ particles obtained by using the sol–gel method according to Ref. [19] is also shown in Fig. 7a. The lattice parameters of all samples are the same to those given in the ICDD card (No. 96-110-1112) [20]. It is seen that all diffraction peaks of $LiFePO_4$/C composite fibers can be indexed to an olivine $LiFePO_4$ with orthorhombic crystal structure (Space Group: Pnma) and there are no impurity phase peaks. Therefore, the $LiFePO_4$ component in composite fibers is phase-pure. The pres-

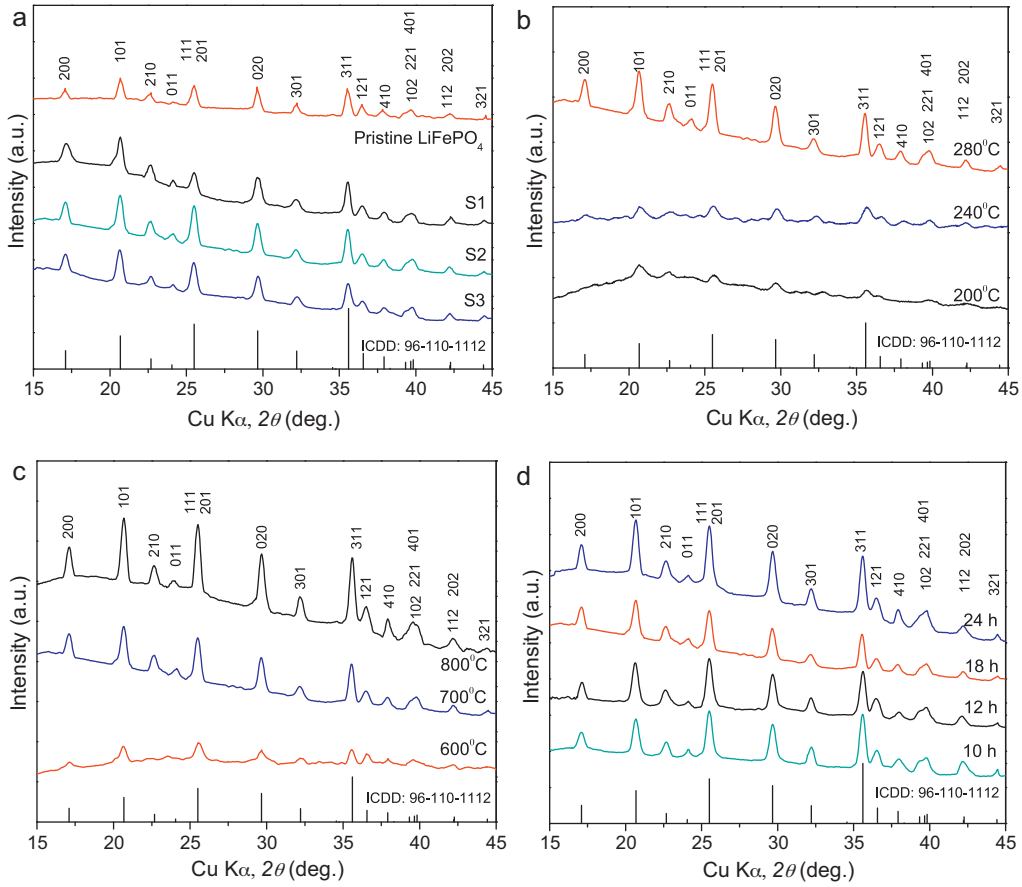

Fig. 7. X-ray diffraction patterns of (a) $LiFePO_4$/C composite fibers obtained from S1, S2, S3 and pristine $LiFePO_4$, (b) $LiFePO_4$/C composite fibers obtained from S2 using different stabilization temperatures, (c) $LiFePO_4$/C composite fibers obtained from S2 using different calcination/carbonization temperatures, and (d) $LiFePO_4$/C composite fibers obtained from S2 using different calcination/carbonization times. The reflections of $LiFePO_4$ (ICDD No. 96-110-1112) are shown in all figures for comparison.

ence of amorphous carbon contributes to the amorphous part in the diffraction pattern of $LiFePO_4$/C composite fibers. From Fig. 7a, the average $LiFePO_4$ crystallite size, which is different than particle size, can be calculated by the Scherrer's equation ($L = 0.9\lambda/\beta\cos\theta$) from the full width at half maximum (FWHM or β) of (2 0 0), (1 0 1), (2 0 1) or (1 1 1), (0 2 0), and (3 1 1) peaks [21]. Crystallite sizes for $LiFePO_4$/C composite fibers prepared from S1, S2 and S3 were found to be 19, 21, and 22 nm, respectively.

Effects of heat-treatment conditions on the structure of $LiFePO_4$/C composite fibers prepared from S2 are shown in Fig. 7b–d. Fig. 7b shows the XRD patterns of $LiFePO_4$/C composite fibers prepared from S2 by using different stabilization temperatures (200, 240 and 280 °C). The calcination/carbonization temperature and time used were 700 °C and 18 h, respectively. It is seen that only low-intensity olivine peaks can be found for samples stabilized at 200 and 240 °C. When the stabilization temperature increases to 280 °C, the peaks become narrower and their intensities increase significantly, indicating increased crystallinity of $LiFePO_4$. Therefore, the appropriate stabilization temperature is 280 °C, which allows the formation of crystallized $LiFePO_4$ olivine phase. Fig. 7c shows the XRD patterns of $LiFePO_4$/C composite fibers prepared from S2 using different calcination/carbonization temperatures (600, 700 and 800 °C for 18 h). The stabilization temperature used was 280 °C. It is seen that the diffraction peaks of all samples can be assigned to the olivine phase. In addition, the peaks become narrower with increase in calcination/carbonization temperature. The crystallite sizes were calculated to be 18, 21, to 28 nm, respectively, when the calcination/carbonization temperatures were 600, 700 and 800 °C. The XRD patterns of $LiFePO_4$/C composite fibers prepared from S2 using a calcination/carbonization temperature of 700 °C for 10, 12, 18 and 24 h are presented in Fig. 7d. It is seen that all four fiber samples contain ordered olivine $LiFePO_4$ with orthorhombic Pnma structure. Crystallite sizes for $LiFePO_4$/C composite fibers obtained at 700 °C for 10, 12, 18 and 24 h were found to be 18, 19, 21 and 25 nm, respectively.

3.3. Electrochemical performance of $LiFePO_4$/C composite fibers

The first charge–discharge curves of $LiFePO_4$/C composite fiber cathodes prepared from three electrospinning solutions (S1, S2 and S3) are illustrated in Fig. 8. The fibers were stabilized at 280 °C for 5 h and calcined/carbonized at 700 °C for 18 h. For fibers prepared from S2 and S3, flat voltage plateaus can be observed between

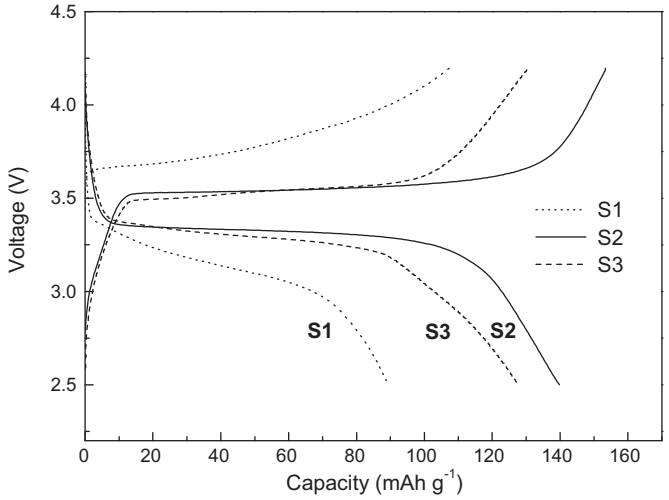

Fig. 8. Initial charge–discharge curves of $LiFePO_4$/C composite fiber cathodes prepared from S1, S2, and S3. Charge–discharge rate: 0.1 C.

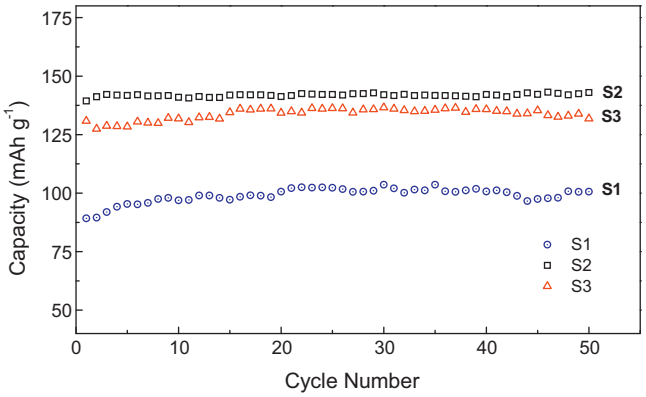

Fig. 9. Cycling performance curves of $LiFePO_4$/C composite fiber cathodes prepared from S1, S2, and S3. Charge–discharge rate: 0.1 C.

3.31–3.54 V and 3.26–3.55 V, which are the main characteristic of the two-phase reaction of $LiFePO_4$. However, fibers prepared from S1 show higher polarization and less flat plateaus between 2.96 and 3.87 V. This phenomenon is directly related to the carbon content in the composite [22,23]. However, as shown in Fig. 6a, higher amount of carbon content results in thicker carbon coating, which prevents penetration of the electrolyte to the active material and leads to higher polarization when the fibers were prepared from S1.

Fig. 9 shows the cycling performances of $LiFePO_4$/C composite fiber cathodes prepared from three electrospinning solutions. It is seen that all three cathodes show good cyclability. Instead of capacity fading, a slight increase in capacity can be observed after several cycles for all three cathodes, which may be attributed to slow electrolyte penetration into the electrode or the crack formation on the amorphous carbon layer during cycling that increases surface area of fibers and improves electrode–electrolyte interaction [6]. From Figs. 8 and 9, it is also seen that $LiFePO_4$/C composite fibers prepared from S2 have higher capacities than those from S1 and S3. Therefore, S2 was used for additional experiments to further improve the electrochemical performance.

3.4. Effect of heat-treatment conditions

Stabilization temperature has great influence on the electrochemical performance of $LiFePO_4$/C composite fibers. Fig. 10 shows the cycling performance of $LiFePO_4$/C composite fibers prepared from S2 using different stabilization temperatures. The stabilization time used was 5 h, and the calcination/carbonization temperature and time were 700 °C and 18 h, respectively. From

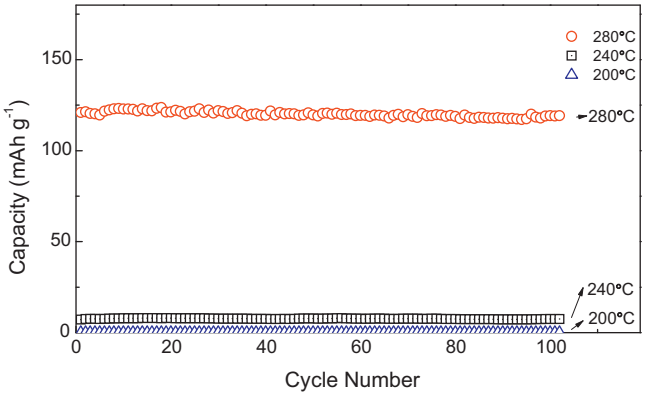

Fig. 10. Effect of stabilization temperature on the discharge capacity of $LiFePO_4$/C composite fibers. Charge–discharge rate: 0.2 C.

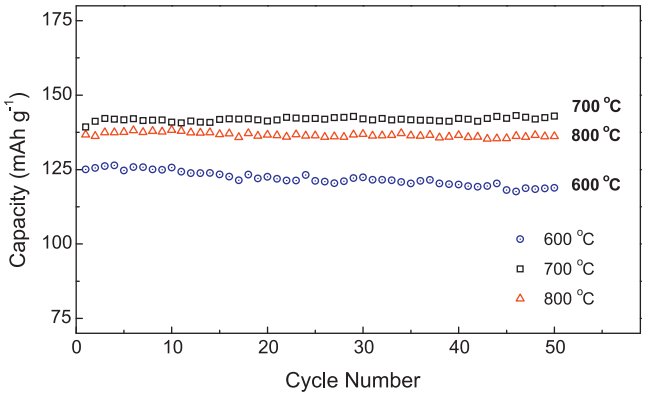

Fig. 11. Effect of calcination/carbonization temperature on the discharge capacity of $LiFePO_4$/C composite fibers. Charge–discharge rate: 0.1 C.

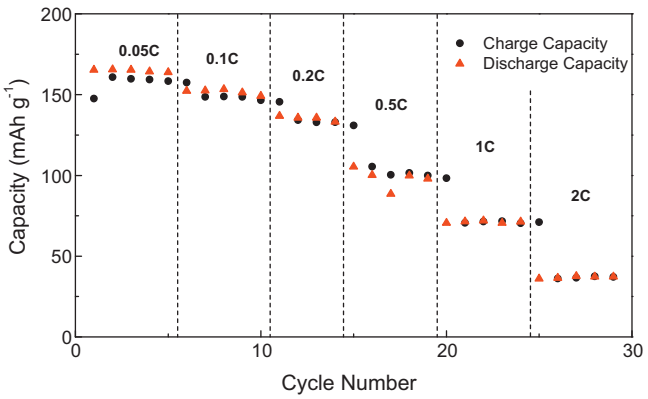

Fig. 13. Rate capability of $LiFePO_4$/C composite fibers. Charge rate: 0.05 C.

Fig. 10, it is seen that $LiFePO_4$/C composite fibers stabilized at 280 °C show discharge capacities of around 125 mAh g^{-1} at 0.2 C. However, fibers stabilized at 200 and 240 °C for 5 h show no useful capacities. This phenomenon can be explained using the XRD data shown in Fig. 7b. When the stabilization temperature was 200 and 240 °C, no sufficient $LiFePO_4$ crystalline structure was formed, and hence the resultant $LiFePO_4$/C composite fibers have low capacities. In addition, stabilization temperatures of 200 and 240 °C are too low for stabilizing PAN to form cyclic rings, and as a result, no sufficient carbon is obtained in the resultant fibers [24–26]. Therefore, the stabilization temperature selected for the following work was 280 °C.

The electrochemical performance of $LiFePO_4$/C composite fibers is also directly affected by the calcination/carbonization temperature [27]. Fig. 11 shows the cycling performance of $LiFePO_4$/C composite fibers stabilized at 280 °C for 5 h and calcined/carbonizaed at 600, 700 and 800 °C, respectively, for 18 h. It is seen that the average discharge capacities are 125, 141 and 136 mAh g^{-1} at 0.1 C for 600, 700 and 800 °C. The best cycling performance is acquired from $LiFePO_4$/C composite fibers calcined/carbonized at 700 °C.

Calcination/carbonization time is another parameter that affects the electrochemical performance of $LiFePO_4$/C composite fibers. In order to investigate the effect of calcination/carbonization time, fibers stabilized at 280 °C for 5 h were further calcined/carbonized at 700 °C for 10, 12, 18 and 24 h, respectively. As shown in Fig. 12, when the calcination/carbonization time ranges between

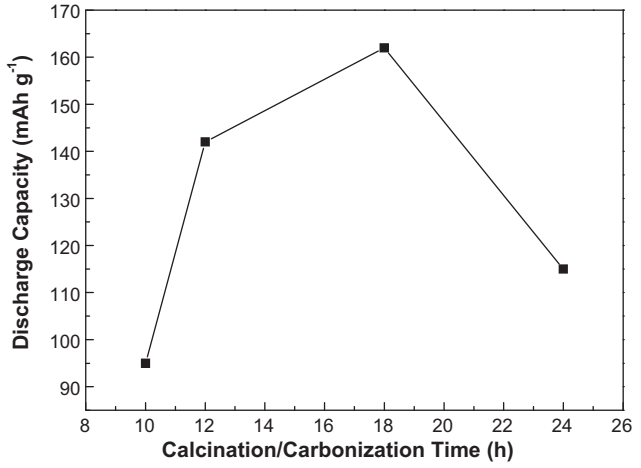

Fig. 12. Effect of calcination/carbonization time on the discharge capacity of $LiFePO_4$/C composite fibers. Charge–discharge rate: 0.05 C.

10 and 18 h, the initial discharge capacity of $LiFePO_4$/C composite fibers increases with increase in calcination/carbonization time. However, with further increase in calcination/carbonization time after 18 h, the discharge capacity of $LiFePO_4$/C composite fibers decreases. As a result, $LiFePO_4$/C composite fibers calcined/carbonized at 700 °C for 18 h delivers the highest capacity of 166 mAh g^{-1} at 0.05 C, which corresponds to 97% of the theoretical capacity.

Based on the results discussed above, it can be concluded that $LiFePO_4$/C composite fibers show the highest capacity and best cycling performance when they are prepared from S2 (8% $LiFePO_4$ precursor/4% PAN solution) by stabilizing at 280 °C for 5 h under air and calcinating/carbonizing at 700 °C for 18 h under argon. Fig. 13 shows the rate capability of these $LiFePO_4$/C composite fibers. During the test, the fibers were charged at 0.05 C, but discharged at different *C*-rates. Average discharge capacities are obtained as 162, 153, 136, 98, 71 and 37 mAh g^{-1}, respectively, for discharge rates of 0.05 C, 0.1 C, 0.2 C, 0.5 C, 1 C and 2 C. Although the rate capability results are relatively good, they are still inadequate for certain applications, such as electrical vehicles (EVs) or hybrid electrical vehicles (HEVs). To overcome this problem, further work is required to increase the electronic and ionic conductivities of the composite fibers. For example, the ionic conductivity of the cathode is as important as the electronic conductivity, and hence research is needed to improve the ionic conductivity of $LiFePO_4$/C composite fibers. Work is also required to reduce the thickness and the amount of carbon in the electrodes to improve the kinetic at higher current densities. In addition, further work will also be focusing on establishing the processing–structure–performance relationships for these novel composite fibers and the use of such fundamental knowledge to achieve high-performance $LiFePO_4$/C composite fibers that can be used in next-generation lithium-ion batteries.

4. Conclusions

Electrospun $LiFePO_4$/C composite fibers with different carbon contents were synthesized and the synthesis conditions were investigated to improve the electrochemical performance. Homogeneously dispersed carbonaceous layer on $LiFePO_4$ and decreased particle size were achieved by electrospinning and subsequent heat-treatment. It was found that among all fibers studied, $LiFePO_4$/C composite fibers electrospun from 8% $LiFePO_4$ precursor/4% PAN solution, stabilized at 280 °C for 5 h under air, and then calcined/carbonized at 700 °C for 18 h under argon, provided the best electrochemical performance. The results demonstrated that electrospinning is a promising approach to prepare high-performance $LiFePO_4$/C composite fibers that have the potential to replace commercial cathodes for lithium-ion batteries.

Acknowledgements

The authors wish to acknowledge the National Textile Center for funding this research. Facilities and resources at the NCSU College of Textiles and the Department of Chemical and Biomolecular Engineering were utilized to complete this research.

References

[1] A.K. Padhi, K.S. Nanjundaswamy, C. Masquelier, S. Okada, J.B. Goodenough, J. Electrochem. Soc. 144 (1997) 1609–1613.
[2] S. Chung, J.T. Bloking, Y. Chiang, Nat. Mater. 1 (2002) 123–128.
[3] P.S. Herle, B. Ellis, N. Coombs, L.F. Nazar, Nat. Mater. 3 (2004) 147–152.
[4] D.Y. Wang, H. Li, S.Q. Shi, X.J. Huang, L.Q. Chen, Electrochim. Acta 50 (2005) 2955–2958.
[5] N. Ravet, Y. Chouinard, J.F. Magnan, S. Besner, M. Gauthier, M. Armand, J. Power Sources 97–98 (2001) 503–507.
[6] R. Dominko, M. Bele, M. Gaberscek, M. Remskar, D. Hanzel, J.M. Goupil, S. Pejovnik, J. Jamnik, J. Power Sources 153 (2006) 274–280.
[7] Z.H. Chen, J.R. Dahn, J. Electrochem. Soc. 149 (2002) A1184–A1189.
[8] C. Delacourt, P. Poizot, S. Levasseur, C. Masquelier, Electrochem. Solid-State Lett. 9 (2006) A352–A355.
[9] D. Jugovic, D. Uskokovic, J. Power Sources 190 (2009) 538–544.
[10] O. Toprakci, H.A.K. Toprakci, L. Ji, X. Zhang, KONA Powder Part. J. 28 (2010) 50–73.
[11] S. Lee, M. Jung, J. Im, K. Sheem, Y. Lee, Res. Chem. Intermediates 36 (2010) 591–602.
[12] E. Hosono, Y. Wang, N. Kida, M. Enomoto, N. Kojima, M. Okubo, H. Matsuda, Y. Saito, T. Kudo, I. Honma, H. Zhou, ACS Appl. Mater. Interfaces 2 (2010) 212–218.
[13] Y. Liang, L. Ji, B. Guo, Z. Lin, Y. Yao, Y. Li, M. Alcoutlabi, Y. Qiu, X. Zhang, J. Power Sources 196 (2011) 436–441.
[14] L. Ji, Z. Lin, R. Zhou, Q. Shi, O. Toprakci, A.J. Medford, C.R. Millns, X. Zhang, Electrochim. Acta 55 (2010) 1605–1611.
[15] L. Ji, Y. Yao, O. Toprakci, Z. Lin, Y. Liang, Q. Shi, A.J. Medford, C.R. Millns, X. Zhang, J. Power Sources 195 (2010) 2050–2056.
[16] Z. Lin, L. Ji, O. Toprakci, W. Krause, X. Zhang, J. Mater. Res. 25 (2010) 1329–1335.
[17] S. Dalton, F. Heatley, P.M. Budd, Polymer 40 (1999) 5531–5543.
[18] M. Gaberscek, R. Dominko, J. Jamnik, Electrochem. Commun. 9 (2007) 2778–2783.
[19] N. Iltchev, Y. Chen, S. Okada, J. Yamaki, J. Power Sources 119–121 (2003) 749–754.
[20] V.A. Streltsov, E.L. Belokoneva, V.G. Tsirelson, N.K. Hansen, Acta Crystallogr. B 49 (1993) 147–153.
[21] G. Arnold, J. Garche, R. Hemmer, S. Strobele, C. Vogler, A. Wohlfahrt-Mehrens, J. Power Sources 119 (2003) 247–251.
[22] R. Dominko, M. Bele, M. Gaberscek, M. Remskar, D. Hanzel, S. Pejovnik, J. Jamnik, J. Electrochem. Soc. 152 (2005) A607–A610.
[23] K. Hsu, S. Tsay, B. Hwang, J. Power Sources 146 (2005) 529–533.
[24] A. Gupta, I.R. Harrison, Carbon 34 (1996) 1427–1445.
[25] A. Gupta, I.R. Harrison, Carbon 35 (1997) 809–818.
[26] K. Suzuki, T. Iijima, M. Wakihara, Electrochim. Acta 44 (1999) 2185–2191.
[27] A.S. Andersson, J.O. Thomas, B. Kalska, L. Haggstrom, Electrochem. Solid-State Lett. 3 (2000) 66–68.